Korean J. Chem. Eng., **16**(6), 856-860 (1999)
SHORT COMMUNICATION

A Simulation of Electrochemical Kinetics for Gas-Liquid-Solid Phase of MCFC Anode

Jun-Heok Lim†, Gyeong Beom Yi, Kuen Hack Suh, Jea-Keun Lee*, Yun Sung Kim and Hai-Soo Chun****

Department of Chemcal Engineering, *Department of Environmental Engineering, Pukyong University, Pusan 608-739, Korea
**Department of Chemcal Engineering, Korea University, Seoul 136-701, Korea
(Received 6 May 1999 • accepted 13 October 1999)

Abstract–A porous Ni-Al alloy anode for the molten carbonate fuel cell has been developed to enhance the creep resistance of the anode as well as to minimize the electrolyte loss. A dual-porosity filmed agglomerate model for the Ni-Al alloy anode has been investigated to predict the cell performance. The major physicochemical phenomena being modeled include mass transfer, ohmic losses and reaction kinetics at the electrode-electrolyte interface. The predicted polarization curves are compared with the experimental results obtained from a half cell test. The model predicted very well the steady-state cell performance at the given conditions that characterize the state of the electrode.

Key words: MCFC, Ni-Al Alloy Anode, Creep Resistance, Agglomerate Model

INTRODUCTION

The Molten Carbonate Fuel Cell (MCFC) is often referred to as a second-generation fuel cell because it is expected to achieve commercialization after the Phosphoric Acid Fuel Cell (PAFC) is available in the marketplace. The MCFC is operated at a relatively higher temperature than PAFC. The higher operation temperature provides higher overall system efficiency and greater flexibility in the use of available fuels. Also, the MCFC does not need any expensive material for its electrodes. The MCFC anode is made of nickel powder that is sintered to a porous electrode with a thickness of 0.5-1.0 mm and porosity of 50-70%. The porous nickel anode has high electric conductivity and stability for molten carbonate, but suffers from creep deformation during the operation of an MCFC stack due to the sintering driving force and the weight of stack itself [Park, 1994].

To eliminate excessive creep of the anode in operation of the MCFC stack, the present state-of-the-art anode is made of a Ni-10% Cr alloy. However, it is lithiated by the carbonate electrolyte (62 mol% Li_2CO_3+38 mol% K_2CO_3), and then it consumes carbonate in the cell. To control the creep deformation, Hitachi has developed an anode that Ni-MgO, Ni-Al solid solution, Ni-Co-Al or Ni-Al intermetallic to nickel powder, respectively. Although the anode inserted Ni-Al solid solution is somewhat creep resistance, it is difficult to produce sub-micron grade Ni-Al intermetallics that can increase creep resistance [Takashima et al., 1992; Kim et al., 1998; Chung et al., 1998].

For higher creep resistance and minimization of electrolyte loss, the Ni-Al alloy anode has been widely tested to replace the Ni-10% Cr alloy lately. A coating method of Al or Cr vapor deposition on nickel anode surface has already been developed. By this coating method, many kinds of Ni-Al intermetallics (Ni_3Al, NiAl, Ni_2Al_3, etc.) are obtained simultaneously and have difficult to understand characteristics of each kind of Ni-Al intermetallic [Chun et al., 1994].

To solve this drawback, we developed a production method of directly sub-micron grade Ni-Al intermetallics in eutectic salts and have manufactured a Ni-Al alloy anode that inserted Ni_3Al of Ni-Al intermetallics in nickel powder [Kim, 1997]. Ni_3Al was selected because of the structural stability and strength of the Ni-Al intermetallics at high temperature based on the information from a previous study [Kim et al., 1999].

In this study, we carry out computational simulation to check the performance of the Ni-Al alloy anode manufactured using the above mentioned Ni_3Al. Because of the lower wettability of pure Ni anode than that of NiO cathode, the dry agglomerate model has been chosen for the simulation of pure Ni anode. But the Ni-Al alloy anode has higher wettability than a pure Ni anode. Therefore, we used the filmed agglomerate model for more exactness in the case of the Ni-Al alloy, and we compared the computational result with the experimental result.

THEORY

The performance of the fuel cell is represented the current density and the available cell potential, as a function of gas flow rates and gas compositions, external load, electrode thickness and pore size of electrode. Brown and Rockett [1966] proposed a composite of thin film and flooded pore model, the so-called agglomerate model. It is assumed that the metallic portion consists of porous agglomerates and electrolyte film-coated agglomerate. Models for a molten carbonate fuel cell electrode have been published by Yuh and Selman [1984], Bergman et al. [1992], Lee et al. [1993], Roh et al. [1996], and Suh et al. [1998]. Park [1994] proved the superior electrode wetta-

†To whom correspondence should be addressed.
E-mail: jhlim@dolphin.pknu.ac.kr

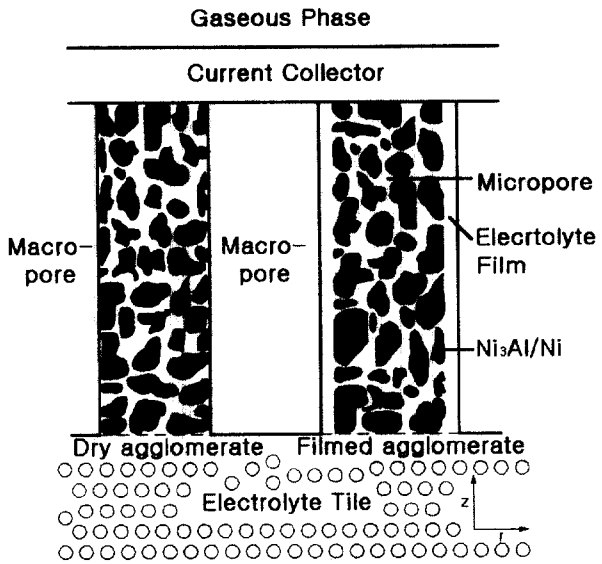

Fig 1. Details of schematic structure of porous electrode in film agglomerate.

bility on molten carbonate electrolyte in the case of the Ni-Al anode. Therefore, we introduce a filmed agglomerate model assuming that electrolyte film is covered macropore and micropore of electrode.

As shown in Fig. 1, the electrode structure can be pictured as one in which catalyst particles form agglomerates which, under working conditions, are flooded with electrolyte. The existence of an electrolyte film of electrolyte on the external surface of the agglomerate depends on the wetting characteristics of the electrolyte on the electrode. It is very likely that such a surface film exists in oxide material (NiO), and intermetallic compound (Ni-Al). Therefore, we have to develop a "Filmed Agglomerate Model" to analyze the Ni-Al alloy anode. Detailed assumptions are described in references [Mitteldorf and Wilemski, 1984]. We will briefly introduce the "filmed agglomerate model" developed by the material balance for reaction gas species i which can be expressed as

$$\nabla \cdot N_i = -\frac{S_i A i_n}{nF} \tag{1}$$

where S_i denotes the stoichiometric coefficient. Also, i_n denotes the transfer current density at the electrode-electrolyte interface due to the electrochemical reaction, and N_i is the mass flux of species i. Applying Fick's law to Eq. (1) in dimensionless cylindrical coordinates Eq. (2) yields:

$$\frac{1}{\xi}\frac{\partial}{\partial\xi}\left(\xi\frac{\partial\bar{C}_i}{\partial\xi}\right)+\frac{R^2}{L^2}\frac{\partial^2\bar{C}_i}{\partial\xi^2}=\frac{R^2 S_i A i_n}{nF\bar{D}_i C_i^b} \tag{2}$$

Where,

$$\bar{C}_i=\left(\frac{C_i}{C_i^b}\right),\ \xi=\left(\frac{r}{R}\right),\ \zeta=\left(\frac{Z}{L}\right) \tag{3}$$

Since the first term is much larger than the second term in Eq. (2), we can neglect the second term. As a result we have Eq. (4)

$$\frac{1}{\xi}\frac{\partial}{\partial\xi}\left(\xi\frac{\partial\bar{C}_i}{\partial\xi}\right)=\frac{R^2 S_i A i_n}{nF\bar{D}_i C_i^b} \tag{4}$$

For S, let the subscripts 1, 2, 3 stand for H_2, CO_2, and H_2O, respectively. The total current output per superficial area (cm^2) is i times the total number of agglomerates per area (cm^2). Since the reference electrode is situated in the electrolyte, the polarization at $x_i=1$ can be known from there. The current density vs. polarization diagram is the final result of this model. With a film on the external surface of the agglomerate, the diffusion Eq. (4) is unchanged within the agglomerates. Due to the diffusion limitation caused by the existence of the film, there is no chemical reaction in the film. One can neglect the axial diffusion term, and the diffusion equations are simply as Eq. (5) in cylindrical coordinates.

$$r\frac{\partial C_i}{\partial r}=\frac{C_i^b-C_i^s}{\Delta}\ \text{where}\ \Delta=\ln\left(\frac{R+\delta}{R}\right) \tag{5}$$

The diffusion flux within the film toward the agglomerate can be computed from Eq. (5). Next, we have to make a material balance at $x_i=1$ to have the appropriate boundary condition over there. For species i, the diffusion flux in the film toward the external surface of agglomerates has to equal to the depletion rate on the external surface plus the diffusion flux toward the interior of the agglomerate. The dimensionless potential equation can be described in Eq. (6) because the current can flow through the film and agglomerate.

$$\frac{d^2\Psi_L}{d\zeta^2}=-\frac{nFD_1C_1^b\phi_L^2}{\kappa R_1(R+\delta)^2\Delta}(1-\bar{C}_i^s) \tag{6}$$

where subscript 1 stands for hydrogen species and R_1 denotes

$$R_1=\left(R^2+\frac{(R+\delta)^2-R^2}{\varepsilon}\right)/(R+\delta)^2$$

At the anode, we can use the Nernst equation [Yuh and Selman, 1984]. If the activities of all species are all zero, the standard equilibrium potential can be obtained by

$$\Psi_a=(V_a^\Phi+\phi_L)\phi \tag{7}$$

Substituting the equation into Eq. (4) gives

$$\frac{1}{\xi}\frac{\partial}{\partial\xi}\left(\xi\frac{\partial\bar{C}_1}{\partial\xi}\right)-\frac{S_1}{S_i}k_i\frac{\partial}{\partial\xi}\left(\xi\frac{\partial\bar{C}_i}{\partial\xi}\right)=0\quad i\neq 1 \tag{8}$$

$$\frac{1}{\xi}\frac{\partial}{\partial\xi}\left(\xi\frac{\partial\bar{C}_1}{\partial\xi}\right)+\left(GI(\bar{C}_1)^{\alpha+\frac{\alpha_a}{2}}(\bar{C}_2)^{\beta-\frac{\alpha_a}{2}}(\bar{C}_3)^{\gamma-\frac{\alpha_a}{2}}\exp(-\alpha_a\Psi_a)\right)$$

$$\left(-GI(\bar{C}_1)^{\alpha+\frac{\alpha_a}{2}}(\bar{C}_2)^{\beta+\frac{\alpha_a}{2}}(\bar{C}_3)^{\gamma+\frac{\alpha_a}{2}}\exp(\alpha_a\Psi_a)\right)=0\quad i=0 \tag{9}$$

where

$$GI=\frac{AR^{2+0}_0}{C_1^b\bar{D}_1(4F)}$$

The potential and current density are related in as Eq. (1)

$$\frac{\partial^2\Psi_a}{\partial\zeta^2}=\frac{-2nFD_1C_1^b\phi L^2}{\kappa R_1(R+\delta)^2\Delta S_1}(1-\bar{C}_1^s) \tag{10}$$

We have three nonlinear coupled partial differential equations which need to be solved by some appropriate numerical method. The potential is only a function of the z-direction. We can

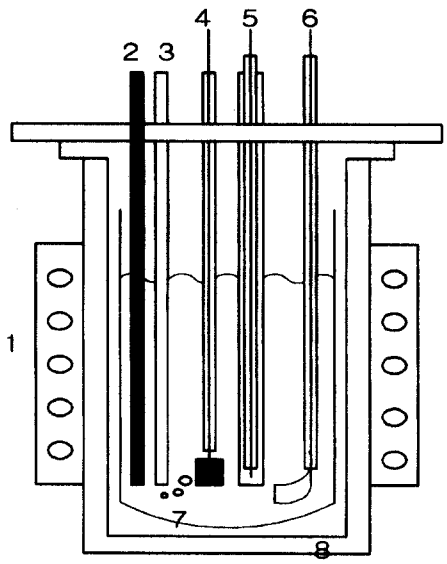

Fig. 2. Schematic diagram of half cell system.

1. Heater
2. Thermocouple
3. Fuel gas inlet
4. Working electrode
5. Reference electrode
6. Counter electrode
7. Alumina crucible
8. Stainless steel

solve the diffusion Eq. (8) and (9) for the anode with a specified value of Ψ_a, depends on z-direction through Eq. (10).

EXPERIMENTAL

We directly synthesized Ni_3Al of Ni-Al intermetallics in (Na+K)Cl eutectic salts by controlling stoichiometric coefficients of reactants, and manufactured the Ni-Al alloy anode inserted Ni_3-Al as discussed in the previous work [Kim, 1997]. A laboratory-scale half cell assembly is used to measure the exchange current density of the Ni-Al alloy anode, as shown in Fig. 2.

The working electrode consisted of pure Ni anode or Ni-Al alloy anode. The counter electrode was made of 99.99% pure gold foil and was bent in a circular shape. These electrodes were connected to 99.99% pure gold wire of 0.5 mm diameter by spot welding. Also, a reference electrode consisted of a 1/8″ alumina tube with a small hole in the bottom that contains carbonate electrolyte and was sparged by gas mixture. The diameter of the hole is 0.5 mm, and its function is to sense the contact between the carbonate in the reference and the working electrode compartment. A $33\%O_2/67\%CO_2$ mixture gas was used as the reference gas. The counter electrode was made of 99.99% pure gold foil and all potentials mentioned were based on a reference electrode.

RESULT AND DISCUSSION

At the beginning of the filmed agglomerate model study, Yuh and Selman [1984] and Lee et al. [1993] calculate the agglomerate radius and the effective surface area by ordered cylinder geometry. It is generally used by other researchers. Though the ordered cylinder geometry is easy to calculate, it is hard to determine the agglomerate size. In comparing the pore size distribution of MCFC anode before and after the experiment, the drastic decrease of micro pore volume in the anode was observed [Chun et al., 1994].

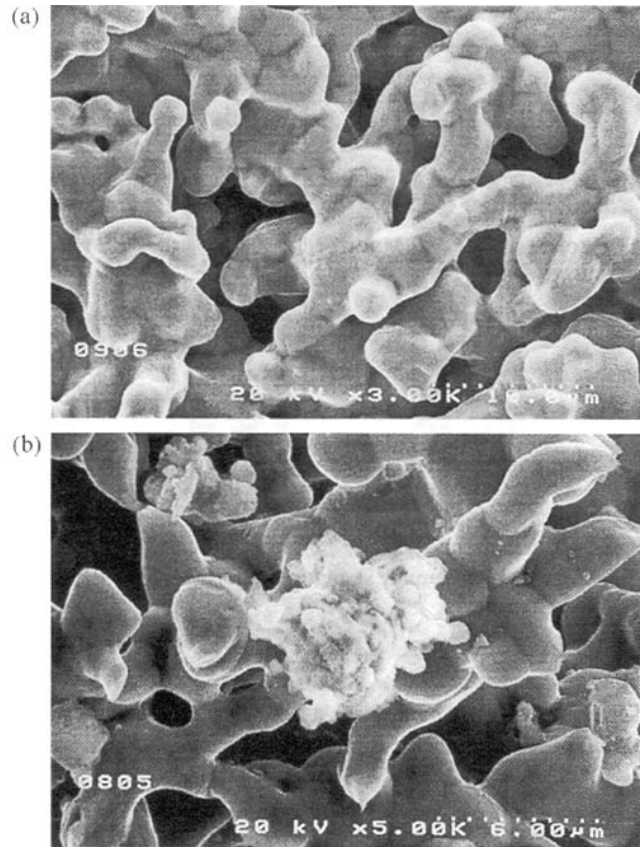

Fig. 3. SEM photographs of the fracture surface in porous MC-FC anodes sintered at 900 °C.

Fig. 3 shows SEM photographs of the fracture surface of MCFC anodes. It is thought that the Ni-Al alloy anode including Ni_3Al has a more stable pore network than pure Ni anode regardless of equal sintering condition. The difference of volume change before and after the cell operation is mainly due to the electrolyte filling in micropore. The wettability of electrolyte in the Ni-Al alloy anode is considerably higher than the Ni anode. During the cell operation, electrolyte might be covering the agglomerate surface and fill micro pore. Thus we can estimate the effective surface area by using the filmed agglomerate model at the hump of cumulative pore volume after the cell operation.

The effect of overpotential and film thickness on the concentration profiles was shown in Fig. 4. Both larger overpotentials and thicker films result in smaller surface hydrogen concentration. A larger overpotential also yields smaller hydrogen concentrations in the core region where film thickness variations have a much smaller influence. The higher the value of film thickness is, the higher the diffusion limitation in the film is. Thicker films may make a lower exchange current density. Because the film is highly conductive, we can expect that the overpotential distribution in the case within film is more uniform than that without film. Thin film increases ohmic resistance and reaction rate, and thereby yields more nonuniform overpo-

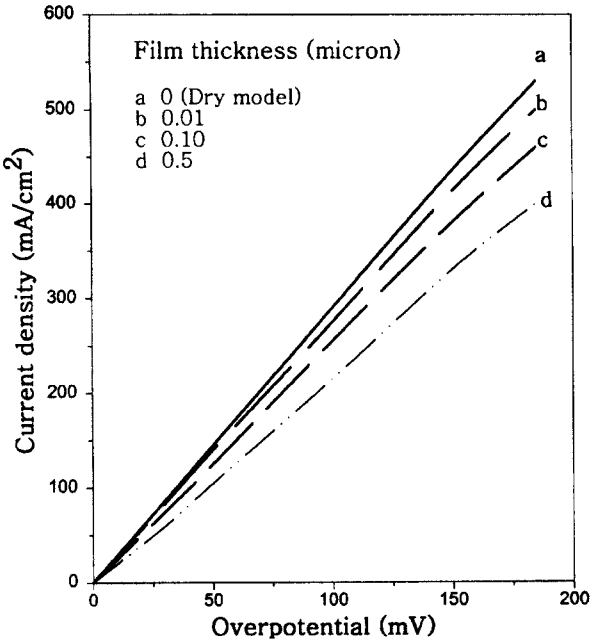

Fig. 4. The effect of carbonate electrolyte film thinkness on the anode performance by filmed agglomerate model.

tential distribution. But the effect is relatively small in this experiment. The high polarization tends to make the overpotential more nonuniform, but this effect may be negligibly small in practical cell operation. It is suggested that a thinner film and a higher exchange current density yield a better electrode performance in agreement with qualitative predictions.

The effect of diffusivity of anode gas on the exchange current density is shown in Fig. 5. Since the effects of diffusivity were approximately of the same order, it seemed that both the activation polarization and diffusion polarization simultaneously controlling step in the Ni-Al alloy anode reaction.

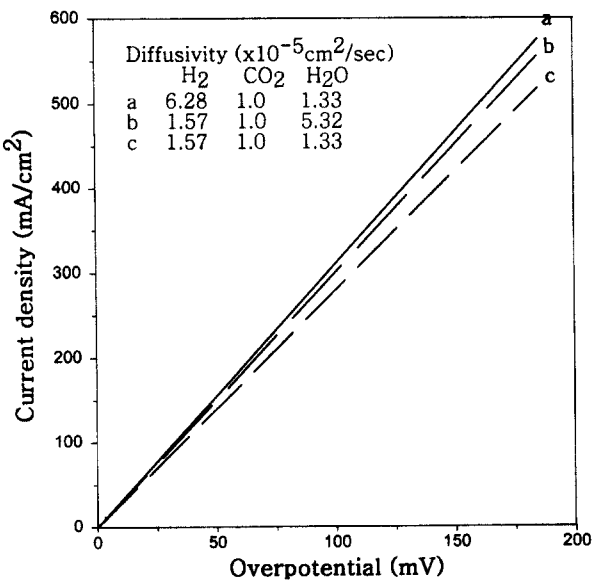

Fig. 5. The effect of anode gas diffusivity on calculated cell performance.

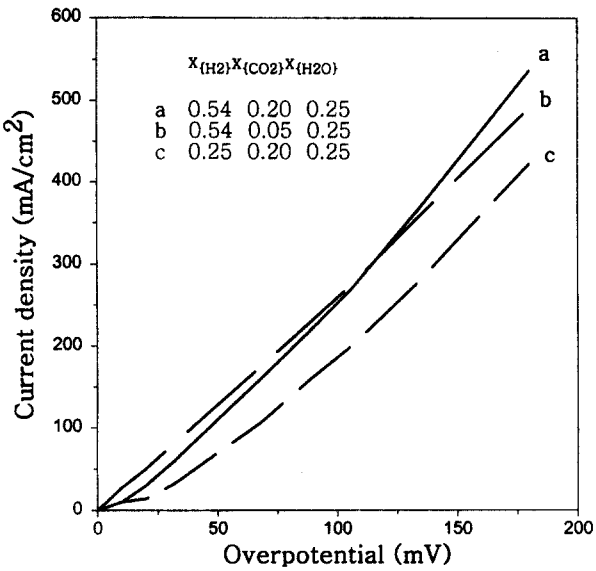

Fig. 6. The effect of gas compositions on calculated Ni-Al alloy anode performance.

Fig. 6 shows the effect of anode gas composition on the exchange current density. As we follow the Ang & Sammells mechanism [Park, 1994], all anodic side gas behaves with the order of 0.25. It shows that the diffusion polarization of each anodic gas makes a difference because they differ from anodic gas in hydrogen and carbon dioxide.

Fitting experimental data to the filmed agglomerate model may be considered as a practical engineering approach to finding the kinetic parameters of hydrogen oxidation in both pure Ni anode and Ni-Al alloy anode. Experimental data from a half cell test using the Ni-Al alloy anode was fitted with the filmed agglomerate model or a dry agglomerate model. In the literature, no film thickness has been experimentally determined yet. The only way to estimate film thickness is to fit the polarization

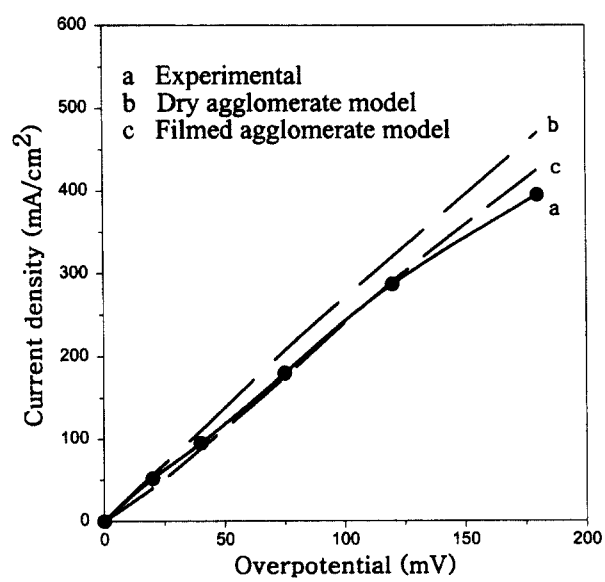

Fig. 7. Comparison of experimental data and predicted IR-free polarization curve of Ni-Al alloy anode.

curve with the lowest gas mole fraction whose limiting current can be determined easily. The film thickness thus determined does not depend on electrode kinetics because the only limitation is the diffusion in the film. In this work, it was assumed that the film thickness determined in this way is independent of gas compositions. This may not be true in practice, but it is a highly convenient assumption in the case of molten carbonate fuel cell electrodes which are practically inaccessible. So the film thickness was calculated by the theory of Mitteldorf and Wilemski [1984].

The experimental data of the half cell test was compared with the theoretical prediction, as shown in Fig. 5. As a result, the filmed agglomerate model appeared to give a better fit than the dry agglomerate model in Ni-Al alloy anode. The dry agglomerate model predicted too high exchange current density.

CONCLUSIONS

The modified filmed agglomerate model combined with the real pore size distribution data gave a good fit to the behavior of a Ni-Al alloy anode. The dry agglomerate model predicts higher current density at a given polarization, whereas the filmed agglomerate model is relatively compatible with experimental data. The Ni-Al alloy anode system needs detailed investigation.

ACKNOWLEDGEMENT

The authors wish to acknowledge the financial support of the Korea Research Foundation made in the program year of 1997.

NOMENCLATURE

A, a : superficial surface area [cm^2]
C_i^b : equilibrium concentration at electrolyte and gas interface [mol/cm^3]
C_i^s : equilibrium concentration at electrode surface [mol/cm^3]
$\bar{D}_i$: effective gas diffusivity [cm^2/s]
F : faraday constant [C/g-eq]
i_L : local current density at electrolyte [A/cm^2]
i_N : exchange current density at anode-electrolyte interface [A/cm^2]
K_i : dissociation constant of species i
L : agglomerate length [cm]
N : agglomerate number [dimensionless]
R, r_o: agglomerate radius [cm]
V_a^ϕ : standard equilibrium potential [V]
Z : axial distance at agglomerate [cm]

Greek Letters

α_a : anodic transfer coefficient [-]
α_c : cathodic transfer coefficient [-]
δ : electrolyte film thickness at agglomerate surface [m]
$\bar{\kappa}$: effective electrolyte conductivity [$1/\Omega cm$]
θ : electrode porosity [dimensionless]
Δ : ln [(R+δ)/R] [dimensionless]
ϕ : F/RT
ϕ_L : potential at electrolyte phase [V]
Ψ_L : $\phi \cdot \phi_L$ [V]
Ψ_a : anodic potential [V]

REFERENCES

Bergman, B., Fontes, E., Lagergren, C. and Simonsson, D., "Mathematical Modelling of the MCFC Cathode," Fuel Cell Seminar Abstract, Tucson, USA (1992).

Brown, R. and Rockett, J. A., "Theory of the Performance of Porous Fuel Cell Electrodes," *J. of Electrochem. Soc.*, **113**, 207 (1966).

Chung, H. C., Park, G. P., Lim, H. C. and Chun, H. S., "Characteristics of Nickel Alloy Anodes for MCFC Prepared by Pack Cementation," *HWAHAK KONGHAK*, **36**, 707 (1998).

Chun, H. S., Park, G. P., Lim, J. H., Kim, K., Lee, J. K., Moon, K. H. and Yoon, J. H., "Pack Aluminization of Nickel Anode for Molten Carbonate Fuel Cell," *J. Power Sources*, **49**, 245 (1994).

Kim, H. J., "Manufacturing Process and Characteristics of Ano-de for MCFC using Ni-Al Intermetallic Powder," MS. Thesis, Korea University, Seoul, Korea (1997).

Kim, H., Nam, S. W., Hong, S. A. and Chung, J. S., "Development of Ni-Al_2O_3 Anodes for Molten Carbonate Fuel Cell," *HWAHAK KONGHAK*, **36**, 856 (1998).

Kim, Y. S., Wee, J. H., Lim, J. H. and Chun, H. S., "Effect of Ni_3Al Intermetallic Compound Inclusion on Ni Grain Growth Inhibition in MCFC Porous Ni-Base Anode," *HWAHAK KONGHAK*, **37**, 97 (1999).

Lee, G. L., Pomp, L. and Selman, J. R., "Comparison of MCFC Cathode Materials by Porous Electrode Performance Modeling," *J. of Electrochem. Soc.*, **140**, 390 (1993).

Mitteldorf, J. and Wilemski, G., "Film Thickness and Distribution of Electrolyte in Porous Fuel Cell Components," *J. of Electrochem. Soc.*, **131**, 1784 (1984).

Park, G. P., "Studies on the Ni-Al Anode for the Molten Carbonate Fuel Cell," Ph.D. Dissertation, Korea University, Seoul, Korea (1994).

Roh, J. S., Hong, S. A. and Suh, S. S., "Effectiveness Factor for Porous Gas Diffusion Electrode of Cylindrical Agglomerate Model with Thin Film," *HWAHAK KONGHAK*, **34**, 663 (1996).

Suh, S. S., Lee, S. J., Nam, S. W., Lim, T. H., Oh, I. H. and Hong, S. A., "Analysis of MCFC Anode Performance," *HWAHAK KONGHAK*, **36**, 144 (1998).

Takashima, S., Ohtsuka, K., Kara, T., Takeuchi, M., Fukui, Y. and Fujimura, H., "Life Issue of Molten Carbonate Fuel Cell," Proceedings of The 1st International Fuel Cell Conference, NEDO/NITI, Tokyo, Japan, **223** (1992).

Yuh, C. Y. and Selman, J. R., "Polarization of the Molten Carbonate Fuel Cell Anode and Cathode," *J. of Electrochem. Soc.*, **131**, 2062 (1984).